Atmos. Chem. Phys. Discuss., 11, 19881–19925, 2011
www.atmos-chem-phys-discuss.net/11/19881/2011/
doi:10.5194/acpd-11-19881-2011

Atmospheric Chemistry and Physics Discussions

Aerosol shortwave daily radiative effect and forcing based on MODIS Level 2 data in the Eastern Mediterranean (Crete)

N. Benas[1], **N. Hatzianastassiou**[2], **C. Matsoukas**[3], **A. Fotiadi**[2], **N. Mihalopoulos**[4], **and I. Vardavas**[1]

[1]Department of Physics, University of Crete, Greece
[2]Department of Physics, University of Ioannina, Greece
[3]Department of Environment, University of the Aegean, Greece
[4]Environmental Chemical Processes Laboratory, Department of Chemistry, University of Crete, Greece

Received: 17 May 2011 – Accepted: 17 June 2011 – Published: 12 July 2011

Correspondence to: N. Benas (benas@physics.uoc.gr)

Published by Copernicus Publications on behalf of the European Geosciences Union.

Abstract

The mean daily shortwave (SW) radiation budget was computed on a 10 km × 10 km resolution above FORTH-CRETE AERONET station in Crete, Greece, for the 9-yr period from 2000 to 2008. The area is representative of the Eastern Mediterranean region, where air pollution and diminishing water resources are exacerbated by high aerosol loads and climate change. The present study aims to quantify the aerosol direct effect and forcing on the local energy budget. A radiative transfer model was used, with daily climatological data from the Moderate Resolution Imaging Spectroradiometer (MODIS), on board NASA's Terra and Aqua satellites. The radiative fluxes were computed at the surface, within the atmosphere and at the top of atmosphere (TOA). Downward surface fluxes and aerosol optical thickness (AOT) were validated against ground measurements. Daily fluxes reveal the direct radiative effects of dust events, with mean daily values reaching up to −100, 55 and −30 W m^{-2} at the surface (cooling), within the atmosphere (warming) and at TOA (cooling), respectively. Mean monthly values show a decreasing trend of the aerosol direct radiative effect, in agreement with a similar trend in AOT. The analysis of the contribution of anthropogenic and natural aerosol show major peaks of natural aerosol direct effect occurring mainly in spring, while a summer maximum is attributed to anthropogenic aerosol. During their peaks, anthropogenic aerosol forcing can reach values of −15 W m^{-2} at the surface, 8 W m^{-2} in the atmosphere and over −4 W m^{-2} at TOA (monthly mean values). The corresponding daily peak values for natural aerosol are over −10 W m^{-2}, 6 W m^{-2} and −3 W m^{-2}. Annual mean values and standard deviations (interannual variability) of anthropogenic aerosol forcing are −10 ± 3 W m^{-2} at the surface, 5 ± 1 W m^{-2} in the atmosphere and −3 ± 1 W m^{-2} at TOA, while the corresponding values for natural aerosol are −6 ± 2 W m^{-2}, 3 ± 1 W m^{-2} and −3 ± 1 W m^{-2}.

ACPD

11, 19881–19925, 2011

1 Introduction

Solar energy, the main source of energy for life on Earth, enters within the Earth-atmosphere system, where it is redistributed. Subsequently, the planet emits radiation back to space at longer wavelengths. The Earth's Radiation Budget (ERB), the result of this procedure, regulates the climate and is an indicator of potential climatic changes. Thus, knowledge and monitoring of the ERB is crucial for improving our understanding of the Earth's climate and its possible changes (IPCC, 2007).

Amongst the different factors that can cause climate change, both greenhouse gases and aerosols play an important role. However, the quantification of the aerosol effects is more complex than the quantification of radiative forcing by greenhouse gases, because aerosol mass and particle number concentrations are highly variable in space and time, due to their much shorter atmospheric lifetime compared with the important greenhouse gases (e.g. Kaufman et al., 2002). Better estimates of the aerosol radiative effects are required to reduce these uncertainties.

To reproduce successfully the distribution of the shortwave (SW) radiation budget through modeling studies on a local or regional scale, a complete description of the processes that govern the transfer of solar radiation within the Earth-atmosphere system is required, together with moderate to high resolution comprehensive data sets for the key surface and atmospheric parameters. The Moderate Resolution Imaging Spectroradiometer (MODIS) instrument, on board NASA's Terra and Aqua satellites, provides most of the data sets needed for modeling the SW effects of aerosols (Chu et al., 2003; King et al., 2003; Remer et al., 2005). MODIS Level 2 data are provided on a daily basis and at 10 km × 10 km latitude-longitude resolution.

Several studies indicate that the aerosol direct radiative effect (DRE) over the Mediterranean is among the highest in the world, especially during summer (Andreae et al., 2002; Formenti et al., 2001). The entire Mediterranean lower troposphere is polluted, although the source regions differ from west to east (Lelieveld et al., 2002; Mihalopoulos et al., 1997). Formenti et al. (2001) and Andreae et al. (2002) related

ACPD
11, 19881–19925, 2011

enhanced aerosol load to transport of air masses from western and eastern Europe and high-altitude transport of mineral dust from northern Africa. Bergamo et al. (2008) examined aerosol properties from six AERONET stations in the Mediterranean and showed that a mixture of anthropogenic and natural aerosols characterize the aerosol load over Crete, in the central-east Mediterranean basin. The studies of Fotiadi et al. (2006) and Kalivitis et al. (2007), also revealed a great variety of aerosol types over the region of Crete, including dust, urban-industrial, biomass-burning pollution and maritime, as well as mixed aerosol types. These aerosol properties, combined with the large solar insolation of the area, make Crete an ideal location to infer the range of aerosol DRE depending on their types.

The present study focuses on the DRE of aerosols, which is the overall effect of natural plus anthropogenic aerosols, and the direct radiative forcing (DRF), which is the effect of anthropogenic aerosols only, on the radiative energy budget. The DRE and forcing of aerosols are computed in the SW range of wavelengths. The corresponding effect is much smaller in the LW (thermal infrared), due to the rapid decrease of aerosol extinction with increasing wavelength for most aerosol types. Even for dust, the thermal infrared radiative effects are about 10 % those for the SW radiation (Tanré et al., 2003). We use MODIS Level 2 Collection 005 data separately from Terra and Aqua satellites, and detailed spectral radiative flux calculations performed with a radiative transfer model. The deterministic radiative transfer model is used to compute the local distribution of all shortwave radiation budget components above FORTH-CRETE AERONET station in Crete, located on the roof of the 20 m-high building of the Hellenic Center for Marine Research (HCMR), which is at 100 m from the coast and 15 km east from Heraklion, the largest city in Crete. The radiation budget components are calculated on a mean daily basis, spanning the 9-yr period from February 2000 through December 2008. The model uses MODIS data for clouds and other surface and atmospheric parameters (see Sect. 3). The data from MODIS are supplemented by aerosol single scattering albedo data, taken from FORTH-CRETE AERONET station, as explained in Sect. 3. The model computations for SW fluxes are validated against

ACPD
11, 19881–19925, 2011

6-yr (2003–2008) measurements from HCMR meteorological station (which is collocated on the northern coast of Crete, with the FORTH-CRETE AERONET station, at 35°19′58″ N, 25°16′55″ E, 20 m altitude), and from Finokalia meteorological station (35°20′ N, 25°40′ E, 150 m altitude, with measurements spanning the period 2001–2007), which is also located at the northern coast of Crete, about 70 km east from Heraklion (Fig. 1). These comparisons ensure the quality of the long-term model results over the wider area, which is a prerequisite for the quality of aerosol DREs and DRFs.

In the next section, the model and the methodology for deriving the aerosol radiative properties are described. Section 3 describes the model input data and the station data used for the validation of the model. The procedure for the validation of MODIS derived Aerosol Optical Thickness (AOT), against FORTH-CRETE AERONET station measurements, along with the model results are given in Sect. 4, before the summary and conclusions.

2 Model description

We use a deterministic spectral radiative transfer model developed from a spectral radiative-convective model (Vardavas and Carver, 1984). Previous, spectral or simpler (broadband) versions of the model have been used by Vardavas and Koutoulaki (1995), Hatzianastassiou and Vardavas (1999, 2001) and Hatzianastassiou et al. (2004a, b, 2005, 2007), to compute the shortwave (SW) radiation budget and the aerosol direct radiative effect on global scales (see also Vardavas and Taylor, 2007).

The incoming solar irradiance at the top of the atmosphere is computed based on the spectral profile of Gueymard (2004), using a solar constant $S_0 = 1367\,\mathrm{W\,m^{-2}}$ (Hartmann, 1994; Willson, 1997) corrected for the Earth's elliptical orbit, as explained by Hatzianastassiou et al. (2004a). The computations are performed separately for 118 wavelengths in the range 0.2–1.0 µm, and 10 spectral bands in the range 1.0–10 µm. For each wavelength and spectral band, a set of monochromatic radiative flux transfer

ACPD
11, 19881–19925, 2011

equations is solved for an absorbing and multiple-scattering atmosphere, using the Delta-Eddington approximation method (Joseph et al., 1976) based on the Henyey-Greenstein phase function, which is an extension of the Eddington method described in Shettle and Weinmann (1970).

The model takes into account physical parameters and processes that affect significantly the solar radiation transfer: absorption by O_3 in the UV region between 0.2 and 0.35 µm (Hartley-Huggins bands) and in the visible, between 0.45 and 0.85 µm (Chappuis bands), and absorption in the near-infrared by water vapor (H_2O), methane (CH_4) and carbon dioxide (CO_2). The model also includes scattering and absorption by clouds and aerosols, Rayleigh scattering and surface reflection. Ozone absorption cross section data are obtained from Sander et al. (2006). Details on the absorption of the molecules considered in the near infrared bands can be found in Vardavas and Taylor (2007) and Vardavas and Carver (1984). Cloud absorption and scattering optical depths are calculated as described in Sect. 3.3, while the corresponding optical depths for aerosols are evaluated using aerosol optical thickness and single scattering albedo data. Computations of the Rayleigh scattering cross sections for the molecules considered are performed as described in Vardavas and Taylor (2007, p. 177).

Depending on the presence of clouds, the atmosphere is divided into different number of layers which determine the solar radiation transfer. Details on this procedure can be found in Vardavas and Koutoulaki (1995) and Hatzianastassiou and Vardavas (1999). Aerosols within and above clouds are not considered in this study, due to missing information. This introduces an underestimate of the aerosol effect in the case of absorbing aerosols above clouds (Keil and Haywood, 2003). In the present study, an aerosol layer above clouds could exist during a Saharan dust event, when the aerosol layer extends up to 7 km in height (Meloni et al., 2005). However, the MODIS algorithm does not retrieve aerosol properties if a cloud is detected (Remer et al., 2005).

Reflection of incident solar radiation from the Earth's surface is taken into account and the surface reflectivity, R_g, is treated as explained by Hatzianastassiou et al. (2004a). In our case, the radiative computations are performed over two

ACPD
11, 19881–19925, 2011

coastal areas. We thus consider two types of surface, land and ocean, so that $R_g = 0.5R_{land} + 0.5R_o$. The ocean reflectivity, R_o, is computed using Fresnel reflection corrected for a non-smooth surface (Vardavas and Taylor, 2007). In the case of land, MODIS Level 2 data products include mean surface reflectance estimated at 7 wavelengths, which is used as input to the model, as explained in Sect. 3.4.

The SW aerosol DRE (denoted henceforth as ΔF) is the direct effect of aerosols on the SW radiation budget at the top of atmosphere (TOA), at the Earth's surface and within the atmosphere, and is given by

$$\Delta F = F - F_{\text{no-aerosol}} \quad (1)$$

where F and $F_{\text{no-aerosol}}$ are the SW radiative fluxes (W m^{-2}) computed with and without aerosols. The computations of the model are based on the shortwave radiation budget of the planet, whereby the net TOA incoming radiation equals the atmospheric plus the surface absorption. Model output includes TOA incoming radiation, TOA outgoing, atmospheric absorption, downwelling SW radiation (DSR), surface absorption and Net TOA incoming radiation. Our evaluation of the DRE emphasizes on the components of the radiation budget, namely the net TOA incoming radiation, the atmospheric absorption and the surface absorption, as well as the DSR, which is a crucial component and can be directly validated against in situ measurements. The DRE components ΔF_{TOA}, ΔF_{atmab}, ΔF_{surf} and $\Delta F_{\text{surfnet}}$, represent the direct effect of aerosols on the net incoming (absorbed) radiation at TOA, within the atmosphere, and at the Earth's surface (DSR and surface absorption). As far as ΔF_{TOA} is concerned, DRE is essentially the change of the outgoing (reflected) SW radiation at TOA, since the incoming extraterrestrial SW radiation is not affected by aerosols, and therefore ΔF_{TOA} will refer to this henceforth, computed according to

$$\Delta F_{\text{TOA}} = F^{\text{TOA}}_{\text{no-aerosol}} - F^{\text{TOA}}. \quad (2)$$

Therefore, positive values of ΔF correspond to decreased outgoing SW radiation at TOA and vice versa.

ACPD
11, 19881–19925, 2011

In the present study, a new version of the model was developed to incorporate the latest available satellite data, namely Level 2 data from the MODIS sensors on board NASA's Terra and Aqua satellites. The model spatial resolution was increased, reaching up to 5 km × 5 km pixel size, depending on the resolution of the MODIS input data. Spatial resolutions of previous versions of the model were 2.5° × 2.5° and 1° × 1° latitude-longitude. The present high spatial resolution offers the possibility of distinguishing patterns that could not be obvious in studies where the resolution was lower, improving also the procedure of model validation against station measurements. The new version is also adjusted to run in two separate modes, one for the evaluation of mean daily results and another for computations regarding the specific satellite overpass time. Results from the first mode only were used in the present study. Modifications were also made to exploit the spectral resolution available from MODIS, regarding aerosol parameters (AOT and asymmetry factor) and the surface reflectance. Aerosol single scattering albedo data from an AERONET station were also incorporated in the present version for the first time. Model input data are described in detail in the next section. Finally, aerosol fine mode fraction, available from MODIS data, was used to separate the DRF from the DRE, as described in Sect. 4.5. The model was run for all days of each year of the study period (February 2000–December 2008). This time period is long enough to allow the examination of possible trends, while the temporal resolution (daily values) allows the evaluation of events characteristic of the aerosol typical life time (e.g. dust events).

3 Model input data

In order to calculate the shortwave radiation budget using the model described above, various atmospheric, cloud and surface properties are required. These are listed in Table 1.

The input data needed are available separately from the Terra and Aqua MODIS instruments, except for the aerosol single scattering albedo, which is taken from the

ACPD
11, 19881–19925, 2011

FORTH-CRETE AERONET Station. MODIS Level 2 Collection 005 data come on a daily basis, at a 10 km × 10 km and 5 km × 5 km resolution for aerosol and all the other data, respectively. The data correspond to the specific overpass time of each satellite, which ranges from 10:20–12:00 for Terra and from 12:40–14:20 for Aqua (local time). MODIS Terra covers the period from February 2000, while MODIS Aqua data are available from July 2002. On the course of the present study, MODIS Level 2 Collection 051 data became available. Comparing all MODIS data used in the model, we found no significant difference between the two Collections.

3.1 Profiles of atmospheric gaseous pollutants and temperature

MODIS provides data of the total O_3 column abundance in Dobson units. For CO_2 a total atmospheric amount is taken equal to $0.59\,g\,cm^{-2}$, corresponding to a fixed mixing ratio of 379 parts per million by volume (ppmv) (2005 value). Similarly, we set the mixing ratios of CH_4 and N_2O equal to 1.774 and 0.319 ppmv, corresponding to 10^{-3} and $4.98 \times 10^{-4}\,g\,cm^{-2}$, respectively (Forster et al., 2007). Specific humidity and atmospheric temperature data are used to compute the total atmospheric water vapor content. The data of atmospheric temperature and dew point temperature, provided by MODIS at surface and at various atmospheric pressure levels up to the stratosphere, are used for the computation of the corresponding specific humidity and temperature profiles.

3.2 Surface properties

MODIS provides all the surface properties required by the model (pressure, temperature and albedo). The land-surface albedo is given at seven wavelengths (0.47, 0.55, 0.66, 0.87, 1.24, 1.64 and 2.13 µm). In order to examine its spectral behavior and intra-annual variability, we have calculated 9-yr seasonal averages from the daily data. Figure 2 shows the mean surface albedo values at the given wavelengths, for the HCMR meteorological station area in Crete, averaged over the 9-yr period 2000–

ACPD
11, 19881–19925, 2011

2008, separately from Terra and Aqua MODIS instruments, for summer (JJA) and winter (DJF) months.

From Fig. 2 it is obvious that Terra and Aqua MODIS data are in general agreement, showing an important spectral variation of surface albedo at the visible and near-IR ranges. A seasonal variation is also apparent, with higher values in the range 0.9–1.4 μm, during summer. The spectral behavior is in very good agreement with the surface reflectivity for vegetation (the station area is surrounded mainly by vegetation), as given in Vardavas and Taylor (2007). The annual vegetation cycle can also explain the observed seasonal variation, as bare soil during the summer months has a higher near-infrared reflectivity than vegetation cover during winter (see Fig. 10.8, Vardavas and Taylor, 2007, p. 359).

3.3 Clouds

All cloud data listed in Table 1, except for the cloud physical thickness, are available from MODIS. Cloud physical thickness was estimated as in Hatzianastassiou and Vardavas (1999). In the present work, we use the ISCCP cloud classification scheme (three cloud types: low, middle and high), adjusted to MODIS data. According to this scheme, cloud data are classified depending on the cloud-top pressure: low-level clouds have top pressures greater than or equal to 680 mbar, high-level cloud-top pressures are less than 440 mbar and middle-level cloud-top pressures lie between 440 and 680 mbar. Specifically, we use the 5 km × 5 km MODIS cloud data pixel covering the station to make the classification and so obtain the cloud properties from the MODIS data.

MODIS provides cloud scattering optical depth, τ_c^s for the wavelengths 0.65 μm over land and 0.86 μm over oceans. For the computation of the cloud shortwave transmissivity and reflectivity in the near-IR, a radiation transfer model also requires cloud absorption as well as scattering optical depth. These were derived from the τ_c^s values given by MODIS, based on Mie computations as described in Hatzianastassiou et al. (2004a) for both liquid and ice clouds. For the UV-visible range, the cloud asymmetry factor is set equal to 0.85 and 0.78 for liquid and ice clouds respectively, while

ACPD
11, 19881–19925, 2011

for the near-IR the corresponding values are 0.82 and 0.80 (Hatzianastassiou et al., 2004a).

3.4 Aerosols

The model requires daily aerosol optical properties, namely AOT, single scattering albedo (ω_{aer}) and asymmetry parameter (g_{aer}). Data of AOT and g_{aer} are provided by MODIS at 7 wavelengths, from 0.47 to 2.13 µm. Data of ω_{aer} are provided by the FORTH-CRETE AERONET station at 4 wavelengths, from 0.44 to 1.02 µm (see Sect. 2). Due to the lack of sufficient measurements from the AERONET station during winter months (November—February), ω_{aer} was obtained by interpolating values from autumn and spring months.

The spectral model computations are performed for specific wavelengths and spectral intervals for the UV-visible and near-IR regions. Thus, the required AOT, ω_{aer} and g_{aer} for these wavelengths and intervals are obtained through interpolation and extrapolation. Finally, the radiative fluxes are computed for each wavelength and spectral interval, with and without aerosols, which are then summed to yield the total SW fluxes, and from their difference the DRE of aerosols.

4 Results

4.1 MODIS AOT validation

MODIS Aerosol algorithm retrieves aerosol optical thickness (AOT or τ_α) at 0.47 and 0.66 µm wavelengths (and interpolates at 0.55 µm) over land surfaces and at seven spectral wavelengths (0.47, 0.55, 0.66, 0.87, 1.2, 1.6, 2.1 µm) over oceans (Kaufman et al., 1997; Tanré et al., 1997). For the comparison database we use AERONET Level 2 data from FORTH-CRETE AERONET station, which are both cloud screened and quality assured (Holben et al., 1998; Dubovik and King, 2000; Dubovik et al., 2000). The AERONET station gives AOT at 0.44, 0.50, 0.67 and 1.02 µm, from direct solar radiation measurements (Holben et al., 2001).

ACPD
11, 19881–19925, 2011

The MODIS Level 2 aerosol products are data sets with a pixel size of 10 km × 10 km at nadir. AERONET AOT data are acquired at 15-min intervals on the average. To achieve a meaningful and balanced validation, we compare spatial statistics from MODIS with corresponding temporal statistics from AERONET (Ichoku et al., 2002). The justification is that, since air masses are constantly in motion, an air mass captured by MODIS across a certain horizontal span over the AERONET site, will be sampled by the sunphotometer during a certain time period.

The basis for the procedure is to identify within each MODIS aerosol image the pixel falling over the station (validation point) by its longitude and latitude. Then an N km × N km subset centered on that pixel is extracted and its mean (μ_s) and standard deviation (σ_s) are computed, where μ_s represents the average value of the parameter, while σ_s expresses its local spatial variability. We tested three window sizes (30 × 30, 50 × 50 and 70 × 70 km) and found that the window-size dependence is generally small and has no specific trend, at least for the window-size range tested. However, we use 50 km × 50 km window-size for calculating all validation spatial statistics, as it is generally adopted and used internationally (Ichoku et al., 2002). For the location of the station identified in the MODIS data, the AERONET sunphotometer data acquired during the 1-h period centered on the MODIS overpass time (± half hour) are extracted. Statistics of the sunphotometer data subsets (mean and standard deviation) are computed. We consider only data subsets computed from a certain minimum number of values (5 pixels out of 25 for MODIS and 2 data points for AERONET). We use the aerosol properties derived from MODIS ocean algorithm, as suggested by Remer et al. (2002), for coastal and island stations.

For the validation, we use AOT values at 675 and 870 nm from FORTH-CRETE AERONET station and at 660 and 865 nm from MODIS Terra and Aqua. These channels are sufficiently similar for direct comparison.

In Fig. 3, the mean values of the 50 km × 50 km MODIS subset and the ±30 min temporal average of the corresponding AERONET timeseries are plotted. The error bars represent the respective spatial and temporal standard deviations. The red line

ACPD
11, 19881–19925, 2011

is the linear regression fit, with the equation, determination coefficient and number of points used shown at the lower right corner. The agreement, as represented by the linear fit, is within the expected uncertainty of the MODIS retrieval algorithm over ocean ($\Delta\tau = \pm 0.03 \pm 0.05\tau$), as denoted by the dotted lines in the figures. The slight overestimation of AOD by MODIS might be partly explained by the slightly smaller observation wavelengths of MODIS than of AERONET. Similar results were obtained by Remer et al. (2002), Ichoku et al. (2002) and Chu et al. (2002), although these studies involved data from several AERONET stations.

4.2 Downwelling SW radiation validation against HCMR and Finokalia station measurements

Aerosol DRE cannot be directly validated against measurements. This can be only indirectly and partly achieved, through validation of DRE components (F, $F_{\text{no-aerosol}}$) and especially of F via comparison against real surface measurements of solar radiation. Figure 4 shows the model results of the daily mean total DSR at HCMR (FORTH-CRETE AERONET) station, against corresponding measurements from the station, for the period 2003–2008, when both station and MODIS data are available. The model was run separately with MODIS Terra (Fig. 4a) and Aqua (Fig. 4b) data as input. The model DSR in both cases is in very good agreement with the ground measurements, as can be seen from the regression fit and the determination coefficients. Nevertheless, there is a bias of $-17\,\mathrm{W\,m^{-2}}$, which corresponds to 6.4 % and 6.5 % of the mean DSR values found, using Terra and Aqua MODIS data, respectively. This trend shows that the model tends to overestimate the DSR at the surface. Figure 5 shows the corresponding results for the DSR at Finokalia station. In this case, the bias is lower ($-13\,\mathrm{W\,m^{-2}}$), corresponding to 4.8 % of the mean output DSR, using Terra and Aqua MODIS input. To investigate the sensitivity of the model overestimation trend to the uncertainty of MODIS AOTs, in the case of HCMR station, we recalculated the DSR, using AOT values computed from the error limits of the MODIS retrieval algorithm ($\tau \pm \Delta\tau$). The two new output datasets were then subtracted from the original model DSR output.

ACPD
11, 19881–19925, 2011

Figure 6 shows the differences in the estimated DSR, when we use the error limits of MODIS AOT retrieval algorithm instead of the AOT values. These differences have values of about 3–4 $W\,m^{-2}$ during summer and drop to 2 $W\,m^{-2}$ in winter, due to overcast conditions, leading either to significantly small AOTs or missing AOT retrievals from MODIS algorithm. Considering this uncertainty, the bias reduces to 4.9 % of the mean DSR values, for both Terra and Aqua MODIS.

Kaufman et al. (2000) showed that at least for aerosols properties, MODIS Terra and Aqua measurements can be regarded as representative of the corresponding daily mean values, although these measurements are acquired at specific times of the day. Figures 7 and 8 show the results of the comparison between Terra and Aqua MODIS AOT at 0.555 µm and between the corresponding model DSR, respectively. In the case of AOT (Fig. 7), Terra MODIS values tend to be greater than Aqua, which can probably be explained by the diurnal cycle of aerosol load in the area. This difference almost disappears in the case of DSR: Fig. 8 seems to verify the statement of Kaufman et al. (2000), at least for the specific site.

4.3 Mean daily time series of aerosol direct radiative effect

Figures 9 and 10 show the daily mean SW aerosol ΔF at the surface ($\Delta F_{\mathrm{Surface}}$), the net surface (surface absorption, $\Delta F_{\mathrm{NetSurface}}$), within the atmosphere ($\Delta F_{\mathrm{AtmAb}}$) and at TOA ($\Delta F_{\mathrm{TOA}}$), for the corresponding years of available MODIS data. The results show that at this site, aerosols cool the Earth – Atmosphere system, by reflecting radiation back to space. They also cool the Earth's surface, while they cause a warming effect within the atmosphere. The aerosol DRE generally takes higher values in summer, due to the larger incoming solar radiation and the clear-sky conditions prevailing during this season. Mean daily values of DRE for the period 2000–2008, calculated from both output data sets (Aqua and Terra MODIS), are given in Table 2.

Dust events, associated with coarse particles transported from African deserts, enhance significantly the aerosol DRE, especially at the surface and within the atmosphere. To further investigate dust events, we first defined them according to the

ACPD
11, 19881–19925, 2011

following criteria: the AOT value should be greater than the mean AOT value for the whole period plus one standard deviation, and the Angstrom exponent less than the corresponding mean value for the whole period minus one standard deviation. Applying the above criteria to both Aqua and Terra MODIS (AOT at 865 nm and Angstrom exponent at 550–860 nm) and AERONET data (AOT at 1020 nm and Angstrom exponent at 440–870 nm), we found several cases when dust events occurred. These cases were further confirmed through back-trajectories, available for the Finokalia station. Back-trajectory calculations were made using the HYSPLIT_4 (Hybrid Single-Particle Lagrangian Integrated Trajectory) modeling system. This public domain model (http://www.arl.noaa.gov/ready/hysplit4.html) is documented in the international literature (Draxler and Hess, 1998). Some of the dust event cases are shown in Table 3, along with the corresponding DRE. Missing values are due to lack of model input data.

During these events, the decrease of surface downwelling radiation can range between −50 and −100 W m^{-2} and the corresponding decrease in surface absorption between −40 and −80 W m^{-2}, while the warming effect within the atmosphere ranges between 30 and 55 W m^{-2}. The outgoing radiation at TOA can be increased by 15 to 25 W m^{-2}.

4.4 Mean monthly time series and trends

To investigate the seasonal characteristics and possible trends of the aerosol DRE during the period examined, we calculated the monthly mean values from the daily means. The results of the monthly mean DRE at the surface (DSR and surface absorption), within the atmosphere and at TOA, are shown in Figs. 11 and 12. Monthly mean DREs that were computed from less than 5 daily mean values are not included in this analysis, to assure that average values are representative for each month. From Fig. 11a it is obvious that the mean monthly aerosol DRE on the DSR can reach up to −30 W m^{-2}, while typical values range between −10 and −20 W m^{-2}. The corresponding monthly mean peak values for the DRE on the radiation absorbed by the surface (Fig. 11b) are −25–−30 W m^{-2}, with a typical range of −5 to −20 W m^{-2}. The DRE

ACPD
11, 19881–19925, 2011

increases the radiation absorbed by the atmosphere (Fig. 12a) by 3 to 10 W m^{-2}, but can reach up to 20 W m^{-2}. At TOA, the result of the DRE is an increase of the outgoing radiation, thus decreasing the net TOA incoming radiation by −4 to −10 W m^{-2} (Fig. 12b). The applied linear regression fits to both time series (from MODIS Terra and Aqua), are also given, along with the computed changes of the DRE ($\Delta y = \Delta(\mathrm{DRE})$), over the period covered from each satellite.

The averaged monthly mean values computed here are in general agreement with the results regarding the wider Mediterranean region from other studies, which combined model simulations and either satellite data or station measurements, although on a global scale and at very lower resolutions (Yu et al., 2004; Takemura et al., 2002; Chou et al., 2002; Remer and Kaufman, 2006).

The computed monthly mean DREs are also in agreement with experimental results, obtained during the MINOS campaign in 2001, when measurements were conducted at Finokalia meteorological station in Crete, about 40 km east of the HCMR station (Markowicz et al., 2002; Satheesh and Ramanathan, 2000). The averaged DRE for summer months at the surface, in the atmosphere and at TOA is in very good agreement with those results, as shown in Table 4. Similar results were also obtained from Matsoukas et al. (2005). In that study, the same model was used, with different input data and resolution, to examine the seasonal Mediterranean Sea heat budget. The July monthly value of the aerosol DRE at the surface was found to be −15 W m^{-2}.

The results of Figs. 11 and 12 also show that almost every year there are two maxima in DRE, one occurring in spring (mainly April) and a secondary in August. This behavior is associated with the corresponding seasonal variation of AOT, which presents high values during these months, due to strong dust episodes taking place in spring and high anthropogenic aerosol load in summer, as was shown by Fotiadi et al. (2006). Table 5 presents the monthly mean AOT values and the corresponding standard deviations from Terra and Aqua MODIS, calculated over the period examined. The results verify this seasonal behavior. This behavior is also obvious if we perform the same trend analysis for the MODIS derived AOT at 0.55 µm, as shown in Fig. 13. The applied

ACPD
11, 19881–19925, 2011

linear fit to the time series of AOT and DRE show that there is a decreasing trend from 2000 to 2008. This trend is in general agreement with the results presented by Papadimas et al. (2008), which showed that there is a decreasing trend of AOT values over the Mediterranean basin, using MODIS Level 3 data and examining the period from 2000 to 2006.

4.5 Contribution of anthropogenic and natural aerosols on DRE

The separation of total aerosol DRE into its natural and anthropogenic components is essential and very important in view of assessing human effects, through emissions of particulate matter (which may also influence natural aerosol events), on the extensively discussed current anthropogenic climate change. To investigate the contribution of anthropogenic (mainly of fine mode) aerosols on the total DRE, we used the following method: for each day, we divided the fine mode AOT given in MODIS data by the total AOT, to calculate the fine mode fraction. For the days that this fraction was greater than 0.7 we assumed that fine mode particles prevailed and that the asymmetry parameter g (taken from MODIS) and single scattering albedo ω (from AERONET) during these days are characteristic of the fine mode. In this section, we used AERONET Level 1.5 single scattering albedo daily values, due to lack of sufficient temporal coverage from Level 2.0. For the days that the fine mode fraction was less than 0.7, we assumed a mixed aerosol load. To separate the anthropogenic component from the total aerosol DRE for days with mixed aerosol load, we also needed values of fine mode g, ω and AOT. While fine mode AOT is already available from MODIS on a daily basis, we used monthly averaged values of fine mode g and ω, computed from the days when the fine mode particles prevailed (fine mode fraction greater than 0.7).

Figure 14 shows the 9-yr mean seasonal total aerosol DRE and DRF at the surface (DSR and surface absorption), within the atmosphere and at TOA, derived using Terra MODIS data, while Fig. 15 shows the corresponding results from Aqua MODIS data. Error bars represent the standard deviation for each month. Higher values of standard deviation generally occur in months with more frequent aerosol events.

ACPD
11, 19881–19925, 2011

The contribution of natural aerosols to DRE was calculated by subtracting the anthropogenic part from the total.

The results from Terra and Aqua are similar, both showing that the contribution from anthropogenic aerosol particles increases during summer and secondarily in spring, presenting maximum values mainly in August and April. Aerosols from natural sources show a different behavior, with a main peak appearing in April. This peak can be attributed to dust events, which occur mainly in spring. The combination of anthropogenic and natural aerosols gives the total DRE, with one peak in spring (April) and one in summer (August). During their peaks, DRF can reach values of $-15\,W\,m^{-2}$ at the surface, $8\,W\,m^{-2}$ in the atmosphere and over $-4\,W\,m^{-2}$ at TOA. The corresponding values for natural aerosol are over $-10\,W\,m^{-2}$, $5\,W\,m^{-2}$ and $-3\,W\,m^{-2}$, respectively. Annual mean values and standard deviations of DRF are $-10 \pm 3\,W\,m^{-2}$ at the surface, $5 \pm 1\,W\,m^{-2}$ in the atmosphere and $-3 \pm 1\,W\,m^{-2}$ at TOA, while the corresponding values for natural aerosol are $-6 \pm 2\,W\,m^{-2}$, $3 \pm 1\,W\,m^{-2}$ and $-3 \pm 1\,W\,m^{-2}$.

5 Summary

We have used a deterministic spectral radiative transfer model, along with various key physical surface and atmospheric parameters, to compute the SW radiation budget and aerosol DRE and DRF at the surface, within the atmosphere and at TOA, above FORTH-CRETE AERONET (HCMR) station in Crete, Greece. The data were taken from the MODIS Level 2 data base (Aerosol, Cloud and Atmospheric Profile Products) and were supplemented with data from FORTH-CRETE AERONET station. The model computations were performed for the 9 yr period from 2000 to 2008, on a mean daily 10 km × 10 km pixel resolution. The results for the DSR were validated against HCMR and Finokalia stations data, showing that in general the model is able to predict the DSR in this region, with a negative bias of about 13 to $17\,W\,m^{-2}$, explained by uncertainties of MODIS AOT product.

ACPD
11, 19881–19925, 2011

The calculated daily mean aerosol DRE at the surface, in the atmosphere and at TOA, showed the significance of dust events in the region, when the DRE at the surface can induce surface cooling as high as $-100\,W\,m^{-2}$. The maximum values observed, of warming and cooling effects in the atmosphere and at TOA, are approximately 70 and $-25\,W\,m^{-2}$, respectively. These large DRE values constitute an important modification factor of the local radiation budget which, given the key location of Crete island, is representative of the eastern or the entire Mediterranean basin. DRE shows a seasonal pattern, with maximum values during spring, following the corresponding increase of AOT, which is caused by the transportation of African dust that occurs mainly in this season. Nevertheless, a secondary maximum is also observed in summer, associated with anthropogenic aerosols.

The linear regression analysis applied to the monthly mean DRE and the AOT reveals a decreasing trend during the period examined, which is in agreement with similar previous results (Papadimas et al., 2008).

The contribution of anthropogenic aerosols is higher during spring and summer (April and August), while that from natural sources (mainly dust events) peaks mainly in spring.

In the future, the current version of the model could be used at various sites of specific interest, regarding the direct effect of aerosols on the radiation budget, to investigate the local patterns of the DRE. This is important, especially in view of the assessment of aerosol DRE and DRF under different aerosol regimes, for example urban, remote continental, biomass burning or desert dust. Such future model computations can also benefit from the increased availability of vertically resolved aerosol information, provided by modern platforms like CALIPSO and CloudSat of A-train satellites. It is also very important to perform validations of computed fluxes against ground stations and satellite measurements, to ensure the validity of the results.

Acknowledgements. This work was supported in part by the Latsis Foundation and IP project CIRCE funded by EU.

ACPD
11, 19881–19925, 2011

References

Andreae, T. W., Andreae, M. O., Ichoku, C., Maenhaut, W., Cafmeyer, J., Karnieli, A., and Orlovsky, L.: Light scattering by dust and anthropogenic aerosol at a remote site in the Negev desert, Israel, J. Geophys. Res., 107(D2), 4008, doi:10.1029/2001JD900252, 2002.

Allen, C. W.: Astrophysical Quantities, 3rd ed., The Athlone Press, University of London, 1976.

Bergamo, A., Tafuro, A. M., Kinne, S., De Tomasi, F., and Perrone, M. R.: Monthly-averaged anthropogenic aerosol direct radiative forcing over the Mediterranean based on AERONET aerosol properties, Atmos. Chem. Phys., 8, 6995–7014, doi:10.5194/acp-8-6995-2008, 2008.

Bryant, C., Eleftheriadis, K., Smolik, J., Zdimal, V., Mihalopoulos, N., and Colbeck, I.: Optical properties of aerosols over the eastern Mediterranean, Atmospheric Environment, 40(32), 6229–6244, 2006.

Chou, M.-D., Chan, P.-K., and Wang, M.: Aerosol radiative forcing derived from SeaWiFS-retrieved aerosol optical properties, J. Atmos. Sci., 59, 748–757, 2002.

Christopher, S. A. and Zhang, J.: Shortwave aerosol radiative forcing from MODIS and CERES observations over the oceans, Geophys. Res. Lett., 29, 1859, doi:10.1029/2002GL014803, 2002.

Chu, D. A., Kaufman, Y. J., Zibordi, G., Chern, J. D., Mao, J., Li, C., and Holben, B. N.: Global monitoring of air pollution over land from the Earth Observing System-Terra Moderate Resolution Imaging Spectroradiometer (MODIS), J. Geophys. Res., 108, 4661, doi:10.1029/2002JD003179, 2003.

Draxler, R. R. and Hess, G. D.: An overview of the HYSPLIT_4 modelling system for trajectories, dispersion and deposition, Aust. Meteorol. Mag., 47, 295–308, 1998.

Dubovik, O. and King, M. D.: A flexible inversion algorithm for retrieval of aerosol optical properties from Sun and sky radiance measurements, J. Geophys. Res., 105, 20673–20696, doi:10.1029/2000JD900282, 2000.

Dubovik, O., Smirnov, A., Holben, B. N., King, M. D., Kaufman, Y. J., Eck, T. F., and Slutsker, I.: Accuracy assessments of aerosol optical properties retrieved from Aerosol Robotic Network (AERONET) Sun and sky radiance measurements, J. Geophys. Res., 105, 9791–9806, doi:10.1029/2000JD900040, 2000.

Formenti, P., Andreae, M. O., Andreae, T. W., Galani, E., Vasaras, A., Zerefos, C., Amiridis, V., Orlovsky, L., Karnieli, A., Wendisch, M., Wex, H., Holben, B. N., Maenhaut, W., and Lelieveld,

ACPD
11, 19881–19925, 2011

J.: Aerosol optical properties and large-scale transport of air masses: Observations at a coastal and a semiarid site in the eastern Mediterranean during summer 1998, J. Geophys. Res., 106, 9807–9826, doi:10.1029/2000JD900609, 2001.

Forster, P., Ramaswamy, V., Artaxo, P., Berntsen, T., Betts, R., Fahey, D. W., Haywood, J., Lean, J., Lowe, D.C., Myhre, G., Nganga, J., Prinn, R., Raga, G., Schulz, M., and Van Dorland, R.: Changes in Atmospheric Constituents and in Radiative Forcing, in: Climate Change 2007: The Physical Science Basis. Contribution of Working Group I to the Fourth Assessment Report of the Intergovernmental Panel on Climate Change, edited by: Solomon, S., Qin, D., Manning, M., Chen, Z., Marquis, M., Averyt, K. B., Tignor, M., and Miller, H. L., Cambridge University Press, Cambridge, United Kingdom and New York, NY, USA, 2007.

Fotiadi, A., Hatzianastassiou, N., Drakakis, E., Matsoukas, C., Pavlakis, K. G., Hatzidimitriou, D., Gerasopoulos, E., Mihalopoulos, N., and Vardavas, I.: Aerosol physical and optical properties in the Eastern Mediterranean Basin, Crete, from Aerosol Robotic Network data, Atmos. Chem. Phys., 6, 5399–5413, doi:10.5194/acp-6-5399-2006, 2006.

Gueymard, C.: The Sun's total and spectral irradiance for solar energy applications and solar radiation models, Solar Energy, 76(4), 423–453, 2004.

Hartman, D. L.: Global Physical Climatology, Academic Press, 411 pp., 1994.

Hatzianastassiou, N. and Vardavas, I.: Shortwave radiation budget of the Northern Hemisphere using International Satellite Cloud Climatology Project and NCEP/NCAR climatological data, J. Geophys. Res., 104, 24401–24421, 1999.

Hatzianastassiou, N. and Vardavas, I.: Shortwave radiation budget of the Southern Hemisphere using ISCCP C2 and NCEP/NCAR climatological data, J. Climate, 14, 4319–4329, 2001.

Hatzianastassiou, N., Fotiadi, A., Matsoukas, Ch., Pavlakis, K., Drakakis, E., Hatzidimitriou, D., and Vardavas, I.: Long-term global distribution of earth's shortwave radiation budget at the top of atmosphere, Atmos. Chem. Phys., 4, 1217–1235, doi:10.5194/acp-4-1217-2004, 2004a.

Hatzianastassiou, N., Katsoulis, B., and Vardavas, I.: Global distribution of aerosol direct radiative forcing in the ultraviolet and visible arising under clear skies, Tellus, 56B, 51–71, 2004b.

Hatzianastassiou, N., Matsoukas, C., Fotiadi, A., Pavlakis, K. G., Drakakis, E., Hatzidimitriou, D., and Vardavas, I.: Global distribution of Earth's surface shortwave radiation budget, Atmos. Chem. Phys., 5, 2847–2867, doi:10.5194/acp-5-2847-2005, 2005.

Hatzianastassiou, N., Matsoukas, C., Fotiadi, A., P. W. Stackhouse Jr., Koepke, P., Pavlakis, K. G., and Vardavas, I.: Modelling the direct effect of aerosols in the solar near-infrared on a

ACPD
11, 19881–19925, 2011

planetary scale, Atmos. Chem. Phys., 7, 3211–3229, doi:10.5194/acp-7-3211-2007, 2007.
Holben, B. N., Eck, T. F., Slutsker, I., Tanré, D., Buis, J. P., Setzer, A., Vermote, E., Reagan, J. A., Kaufman, Y. J., Nakajima, T., Lavenu, F., Jankowiak, I., and Smirnov, A.: AERONET – A federated instrument network and data archive for aerosol characterization, Remote Sens. Environ., 66(1), 1–16, 1998.
Holben, B. N., Tanré, D., Smirnov, A., Eck, T. F., Slutsker, I., Abuhassan, N., Newcomb, W.W., Schafer, J., Chatenet, B., Lavenue, F., Kaufman, Y. J., Vande Castle, J., Setzer, A., Markham, B., Clark, D., Frouin, R., Halthore, R., Karnieli, A., O'Neill, N. T., Pietras, C., Pinker, R. T., Voss, K., and Zibordi, G.: An emerging ground-based aerosol climatology: Aerosol Optical Depth from AERONET, J. Geophys. Res., 106, 12067–12097, 2001.
Ichoku, C., Chu, D. A., Mattoo, S., Kaufman, Y. J., Remer, L. A., Tanré, V., Slutsker, I., and Holben, B. N.: A spatio-temporal approach for global validation and analysis of MODIS aerosol products, Geophys. Res. Lett., 29(12), 8006, doi:10.1029/2001GL013206, 2002.
IPCC, 2007: Climate Change 2007: The Physical Science Basis. Contribution of Working Group I to the Fourth Assessment Report of the Intergovernmental Panel on Climate Change, edited by: Solomon, S., Qin, D., Manning, M., Chen, Z., Marquis, M., Averyt, K. B., Tignor, M., and Miller, H. L., Cambridge University Press, Cambridge, United Kingdom and New York, NY, USA, 996 pp., 2007.
Joseph, J. H., Wiscombe, W. J., and Weinmann, J. A.: The Delta-Eddington approximation of radiative flux transfer, J. Atmos. Sci., 33, 2452–2459, 1976.
Kalivitis, N., Gerasopoulos, E., Vrekoussis, M., Kouvarakis, G., Kubilay, N., Hatzianastassiou, N., Vardavas, I., and Mihalopoulos, N.: Dust transport over the eastern Mediterranean derived from Total Ozone Mapping Spectrometer, Aerosol Robotic Network, and surface measurements, J. Geophys. Res., 112, D03202, doi:10.1029/2006JD007577, 2007.
Kaufman, Y. J., Tanré, D., Remer, L. A., Vermote, E. F., Chu, A., and Holben, B. N.: Operational remote sensing of tropospheric aerosol over land from EOS moderate resolution imaging spectroradiometer, J. Geophys. Res., 102, 17051–17067, 1997.
Kaufman, Y. J., Holben, B. N., Tanré, D., Slutsker, I., Smirnov, A., and Eck, T. F.: Will Aerosol Measurements from Terra and Aqua Polar Orbiting Satellites Represent the Daily Aerosol Abundance and Properties?, Geophys. Res. Lett., 27(23), 3861–3864, 2000.
Kaufman, Y. J., Tanré, D., and Boucher, O.: A satellite view of aerosols in the climate system, Nature, 419, 215–223, 2002.
King, M. D., Menzel, W. P., Kaufman, Y. J., Tanré, D., Gao, B. C., Platnick, S., Ackerman, S.

ACPD
11, 19881–19925, 2011

A., Remer, L. A., Pincus, R., and Hubanks, P. A.: Cloud and aerosol properties, precipitable water, and profiles of temperature and humidity from MODIS. IEEE T. Geosci. Remote Sens., 41, 442–458, 2003.

Keil, A. and Haywood, J.: Solar radiative forcing by biomass burning aerosol particles during SAFARI-2000: A case study based on measured aerosol and cloud properties, J. Geophys. Res., 108(D13), 8467, doi:10.1029/2002JD002315, 2003.

Kondratyev, K. Y.: Radiation Characteristics of the Atmosphere and the Earth's surface, Amerind, New Delhi, 580 pp., 1973.

Lelieveld, J., Berresheim, H., Borrmann, S., Crutzen, P. J., Dentener, F. J., Fischer, H., Feichter, J., Flatau, P. J., Heland, J., Holzinger, R., Korrmann, R., Lawrence, M. G., Levin, Z., Markowicz, K. M., Mihalopoulos, N., Minikin, A., Ramanathan, V., de Reus, M., Roelofs, G. J., Scheeren, H. A., Sciare, J., Schlager, H., Schultz, M., Siegmund, P., Steil, B., Stephanou, E. G., Stier, P., Traub, M., Warneke, C., Williams, J., and Ziereis, H.: Global Air Pollution Crossroads over the Mediterranean, Science, 298, 5594, 794–799, 2002.

Markowicz, K. M., Flatau, P. J., Ramana, M. V., Crutzen, P. J., and Ramanathan, V.: Absorbing mediterranean aerosols lead to a large reduction in the solar radiation at the surface, Geophys. Res. Lett., 29(20), 1968, doi:10.1029/2002GL015767, 2002.

Matsoukas, C., Banks, A. C., Hatzianastassiou, N., Pavlakis, K. G., Hatzidimitriou, D., Drakakis, E., Stackhouse, P. W., and Vardavas, I.: Seasonal heat budget of the Mediterranean Sea, J. Geophys. Res., 110, C12008, doi:10.1029/2004JC002566, 2005.

Meloni, D., di Sarra, A., Di Iorio, T., and Fiocco, G.: Influence of the vertical profile of Saharan dust on the visible direct radiative forcing, J. Quant. Spectrosc. Ra., 93, 347–413, 2005.

Mihalopoulos, N., Stephanou, E., Pilitsidis, S., Kanakidou, M., and Bousquet, P.: Atmospheric aerosol composition above the Eastern Mediterranean region, Tellus, 49B, 314–326, 1997.

Papadimas, C. D., Hatzianastassiou, N., Mihalopoulos, N., Querol, X., and Vardavas, I.: Spatial and temporal variability in aerosol properties over the Mediterranean basin based on 6-year (2000–2006) MODIS data, J. Geophys. Res., 113, D11205, doi:10.1029/2007JD009189, 2008.

Remer, L. A. and Kaufman, Y. J.: Aerosol direct radiative effect at the top of the atmosphere over cloud free ocean derived from four years of MODIS data, Atmos. Chem. Phys., 6, 237–253, doi:10.5194/acp-6-237-2006, 2006.

Remer, L. A., Tanré, D., Kaufman, Y. J., Ichoku, C., Mattoo, S., Levy, R., Chu, D. A., Holben, B. N., Dubovik, O., Smirnov, A., Martins, J. V., Li, R.-R., and Ahmad, Z.: Validation of MODIS

ACPD
11, 19881–19925, 2011

aerosol retrieval over ocean, Geophys. Res. Lett., 29, MOD03, doi:10.1029/2001GL013204, 2002.
Remer, L. A., Kaufman, Y. J., Tanré, D., Mattoo, S., Chu, D. A., Martins, J. V., Li, R. R., Ichoku, C., Levy, R. C., Kleidman, R. G., Eck, T. F., Vermote, E., and Holben, B. N.: The MODIS aerosol algorithm, products and validation, J. Atmos. Sci., 62(4), 947–973, 2005.
Sander, S. P., Friedl, R. R., Ravishankara, A. R., Golden, D. M., Kolb, C. E., Kurylo, M. J. Molina, J., Moortgat, G. K., Keller-Rudek, H., Finlayson-Pitts, B. J., Wine, P. H., Huie, R. E., and Orkin, V. L.: Chemical Kinetics and Photochemical Data for Use in Atmospheric Studies, Evaluation Number 15, Jet Propulsion Laboratory Publication 06-2, California Institute of Technology, Pasadena, 2006.
Satheesh, S. K. and Ramanathan, V.: Large differences in tropical aerosol forcing at the top of the atmosphere and Earth's surface, Nature, 405, 60–63, 2000.
Shettle, E. P. and Weinmann, J. A.: The transfer of solar irradiance through inhomogeneous turbid atmospheres evaluated by Eddington's approximation, J. Atmos. Sci., 27, 1048–1055, 1970.
Takemura, T., Nakajima, T., Dubovik, O., Holben, B., and Kinne, S.: Single-scattering albedo and radiative forcing of various aerosol species with a global three-dimensional model, J. Climate, 15(4), 333–352, 2002.
Tanré, D., Kaufman, Y. J., Herman, M., and Mattoo, S.: Remote sensing of aerosol properties over oceans using the MODIS/EOS spectral radiances, J. Geophys. Res., 102, 16971–16988, 1997.
Tanré, D., Haywood, J., Pelon, J., Leon, J. F, Chatenet, B., Formenti, P., Francis, P., Goloub, P., Highwood, E. J., and Myhre, G.: Measurement and modelling of the Saharan dust radiative impact: Overview of the Saharan Dust Experiment (SHADE), J. Geophys. Res., 108(D18), 8574, doi:10.1029/2002JD003273, 2003.
Vardavas, I. and Carver, J. H.: Solar and terrestrial parameterizations for radiative convective models, Planet. Space Sci., 32, 1307–1325, 1984.
Vardavas, I. M. and Koutoulaki, K.: A model for the solar radiation budget of the Northern Hemisphere: Comparison with Earth Radiation Budget Experiment data, J. Geophys. Res., 100, 7303–7314, 1995.
Vardavas, I. M. and Taylor, F. W.: Radiation and Climate, International Series of Monographs on Physics, 138, Oxford University Press, Oxford, UK, 2007.
Willson, R. C.: Total solar irradiance trend during solar cycles 21 and 22, Science, 277, 1963–

ACPD
11, 19881–19925, 2011

1965, 1997.

Yu, H., Dickinson, R. E., Chin, M., Kaufman, Y. J., Zhou, M., Zhou, L., Tian, Y., Dubovik, O., and Holben, B. N.: Direct radiative effect of aerosols as determined from a combination of MODIS retrievals and GOCART simulations, J. Geophys. Res., 109, D03206, doi:10.1029/2003JD003914, 2004.

ACPD

11, 19881–19925, 2011

Table 1. Input data required to model the shortwave radiation budget.

Cloud Properties	Atmospheric Properties	Surface Properties
Cloud amount	Temperature	Pressure
Cloud scattering optical depth	Specific humidity	Temperature
Cloud absorption optical depth	Atmospheric gases	Albedo
Cloud-top pressure	Aerosol optical depth	
Cloud physical thickness	Aerosol asymmetry parameter	
Cloud phase	Aerosol single scattering albedo	

ACPD
11, 19881–19925, 2011

Table 2. Mean daily values with standard deviations of DRE for the period 2000–2008, calculated from both output data sets (Aqua and Terra MODIS).

	DRE (W m^{-2})
Surface	-15 ± 9
Surface Absorption	-13 ± 8
Atmospheric Absorption	6 ± 5
TOA	-6 ± 3

ACPD
11, 19881–19925, 2011

Table 3. Characteristic dates of dust events and corresponding DRE ($W\,m^{-2}$) at the surface, within the atmosphere, at TOA and net surface.

DRE($W\,m^{-2}$) Date	Surface		Atmosphere		TOA		Net Surface	
	Terra	Aqua	Terra	Aqua	Terra	Aqua	Terra	Aqua
29/03/2003	−99		53		−28		−81	
28/02/2004	−50		24		−17		−41	
27/03/2004		−67		33		−20		−53
29/03/2004		−59		31		−15		−46
18/06/2004		−59		26		−22		−48
26/01/2005	−31	−58	11	24	−14	−21	−26	−45
28/02/2005		−43		20		−15		−35
12/04/2005	−56		28		−19		−47	
26/02/2006		−32		13		−14		−27
10/06/2007	−73	−38	34	17	−22	−13	−56	−30
02/11/2007	−29		12		−13		−24	

ACPD
11, 19881–19925, 2011

Table 4. Model mean aerosol DRE for summer months for the period 2000–2008 as computed in this study, compared with experimental results. The radiative effect is expressed in W m^{-2}.

	Model		Markowicz et al. (2002)
	MODIS/Terra	MODIS/Aqua	
Net Surface	−14 ± 3	−14 ± 2	−18 ± 2
Atmosphere	8 ± 2	8 ± 2	11 ± 4
TOA	−7 ± 1	−7 ± 1	−7 ± 2

ACPD
11, 19881–19925, 2011

Table 5. Monthly mean AOT and standard deviation from Terra and Aqua MODIS, calculated for the period 2000–2008.

Month	Terra MODIS AOT	Aqua MODIS AOT
January	0.132 ± 0.039	0.132 ± 0.032
February	0.182 ± 0.014	0.250 ± 0.153
March	0.262 ± 0.110	0.282 ± 0.096
April	0.290 ± 0.064	0.357 ± 0.133
May	0.252 ± 0.046	0.230 ± 0.032
June	0.202 ± 0.059	0.203 ± 0.027
July	0.216 ± 0.049	0.206 ± 0.034
August	0.230 ± 0.051	0.205 ± 0.037
September	0.224 ± 0.052	0.199 ± 0.018
October	0.223 ± 0.051	0.197 ± 0.038
November	0.182 ± 0.034	0.164 ± 0.025
December	0.159 ± 0.055	0.150 ± 0.036

ACPD
11, 19881–19925, 2011

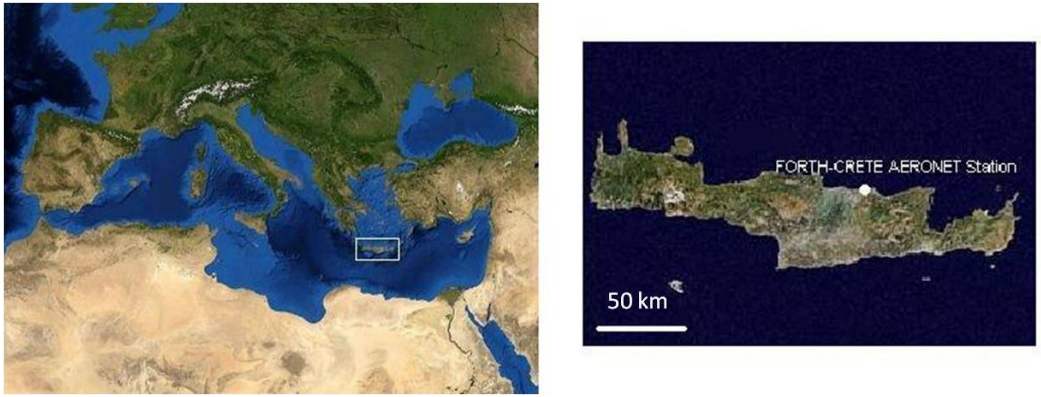

Fig. 1. The Mediterranean basin and the sites of FORTH-CRETE AERONET and Finokalia Stations, on the island of Crete.

ACPD
11, 19881–19925, 2011

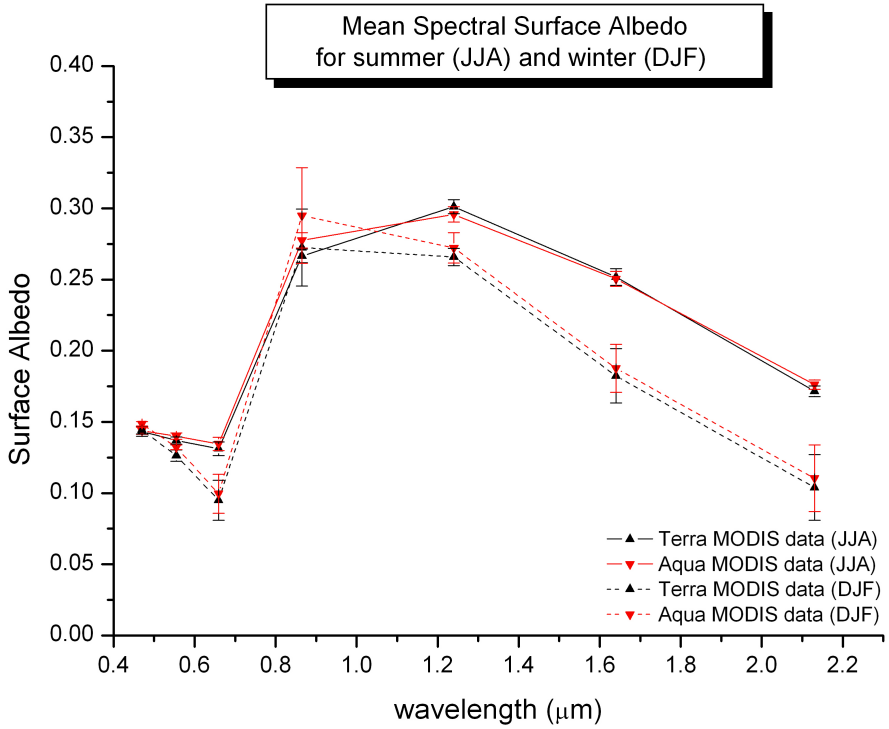

Fig. 2. Mean land-surface albedo at 7 wavelengths, derived from Terra and Aqua MODIS instruments, for the summer (JJA) and winter (DJF) months of the 9-yr period 2000–2008, at the HCMR station in Crete. Error bars represent the standard deviation for each wavelength.

ACPD
11, 19881–19925, 2011

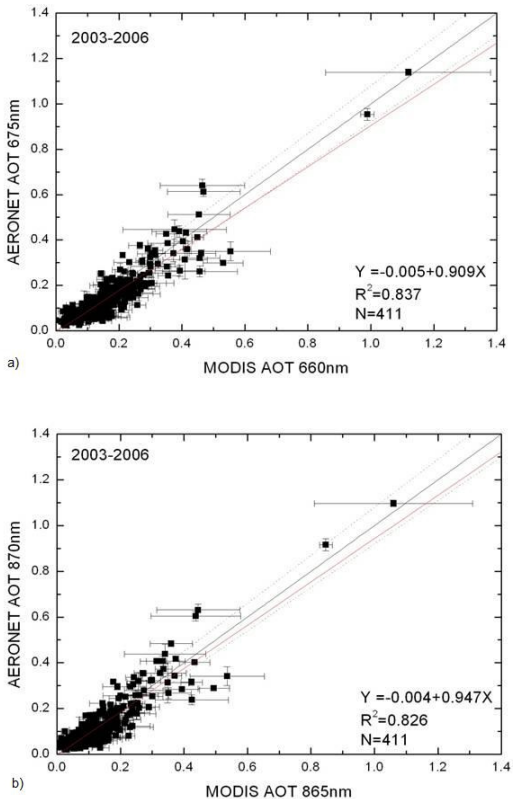

Fig. 3. Scatter plots of means of AOT (660 nm **a** and 865 nm **b**) of MODIS 50 × 50 km subsets against AOT (675 nm **a** and 870 nm **b**) of AERONET 1-h subsets for the period 2003–2006. The error bars represent the respective standard deviations. The red line is the linear regression fit, with the equation, determination coefficient and number of points used shown at the lower right corner. The dotted lines correspond to the expected uncertainty of the MODIS retrieval algorithm.

ACPD
11, 19881–19925, 2011

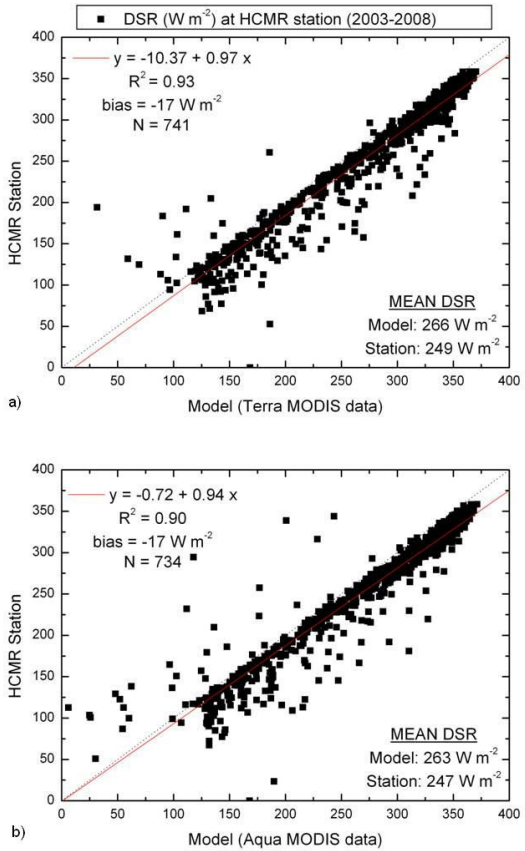

Fig. 4. Scatter plots of the model daily mean DSR using MODIS Terra **(a)** and Aqua **(b)** data, against corresponding ground measurements from HCMR station, for the years 2003–2008. The lines are the linear regression fits, with the equations, determination coefficients, biases, number of points and mean DSR values shown.

ACPD
11, 19881–19925, 2011

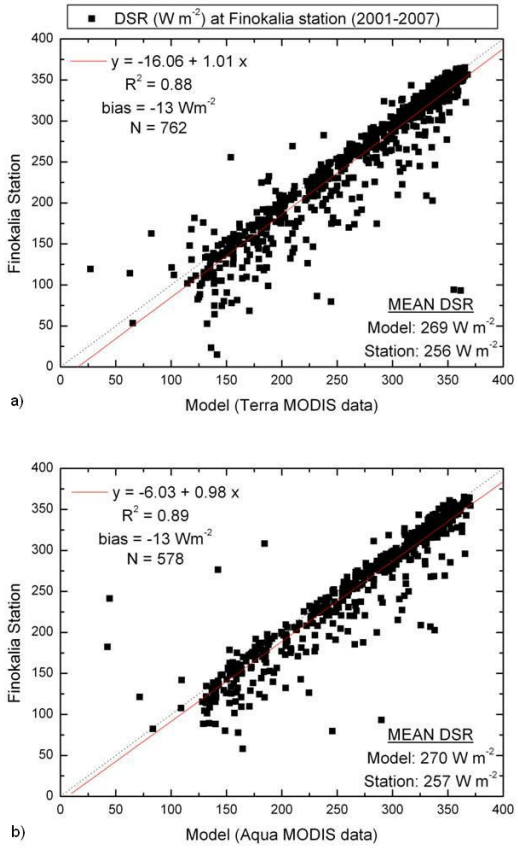

Fig. 5. Scatter plots of the model daily mean DSR using MODIS Terra **(a)** and Aqua **(b)** data, against corresponding ground measurements from Finokalia station, for the years 2001–2007. The lines are the linear regression fits, with the equations, determination coefficients, biases, number of points and mean DSR values shown.

ACPD
11, 19881–19925, 2011

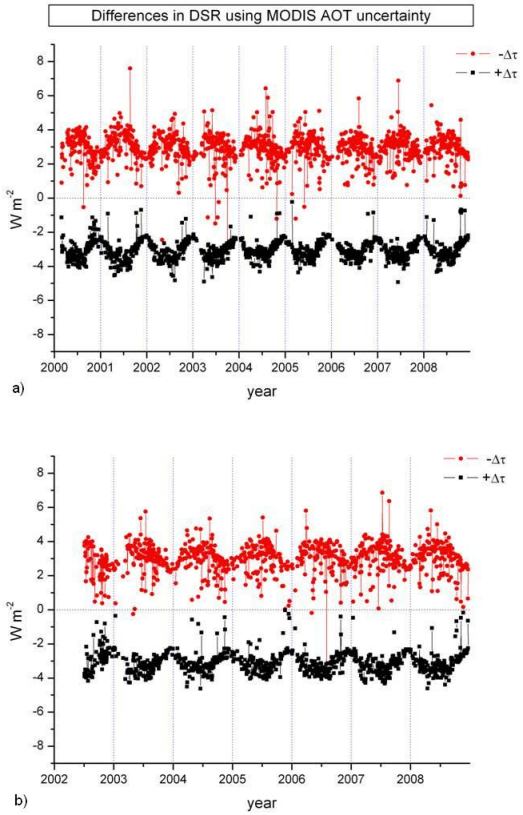

Fig. 6. Timeseries of the differences in model daily mean DSR ($W\,m^{-2}$), using Terra **(a)** and Aqua **(b)** MODIS AOT data and the error limits of the AOT retrieval algorithm ($\tau \pm \Delta\tau$), above HCMR station, for the years 2003–2008.

ACPD
11, 19881–19925, 2011

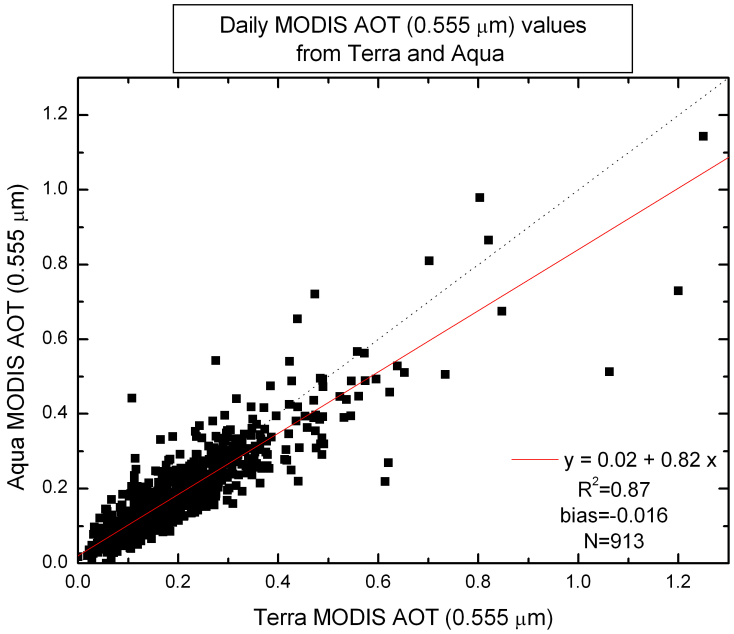

Fig. 7. Scatter plot of the AOT at 0.555 µm, using Terra MODIS data, against corresponding values from Aqua MODIS, for the years 2002–2008. The red line is the linear regression fit, with the equation, determination coefficient, bias and number of points shown at the lower right corner.

ACPD
11, 19881–19925, 2011

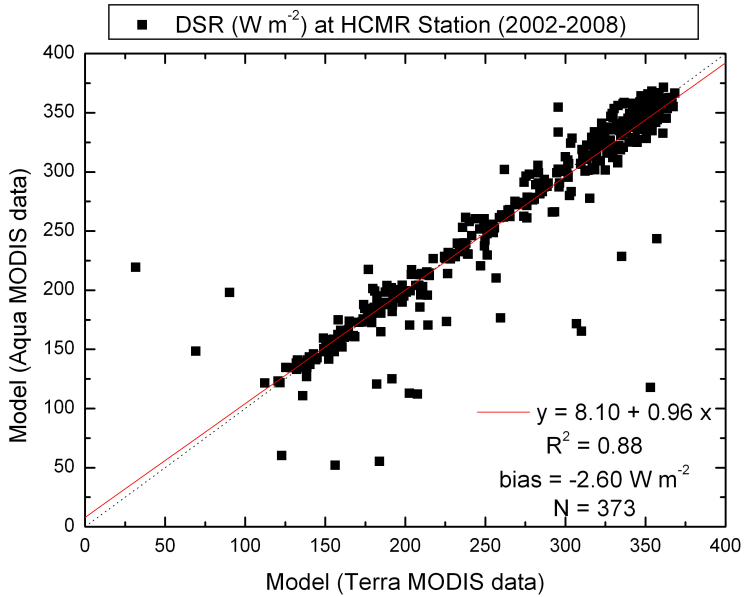

Fig. 8. Scatter plot of the model DSR, using Terra MODIS data, against corresponding values from Aqua MODIS data, for the years 2003–2008. The red line is the linear regression fit, with the equation, determination coefficient, bias and number of points shown at the lower right corner.

ACPD
11, 19881–19925, 2011

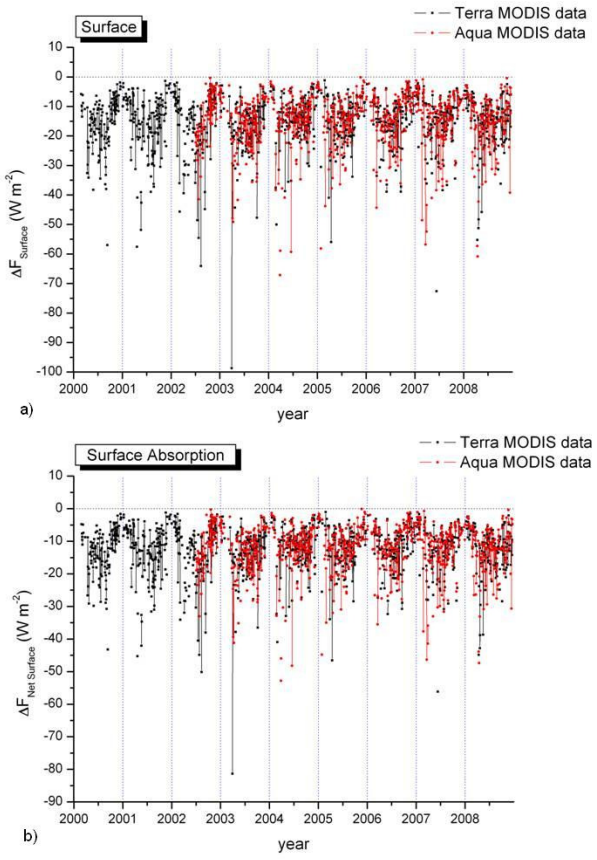

Fig. 9. Time series of the daily mean aerosol effect at the surface (incident **(a)** and absorbed **(b)** radiation), as computed from the model, based on MODIS Level 2 Terra and Aqua data, for the period 2000–2008, at HCMR station, Crete.

ACPD
11, 19881–19925, 2011

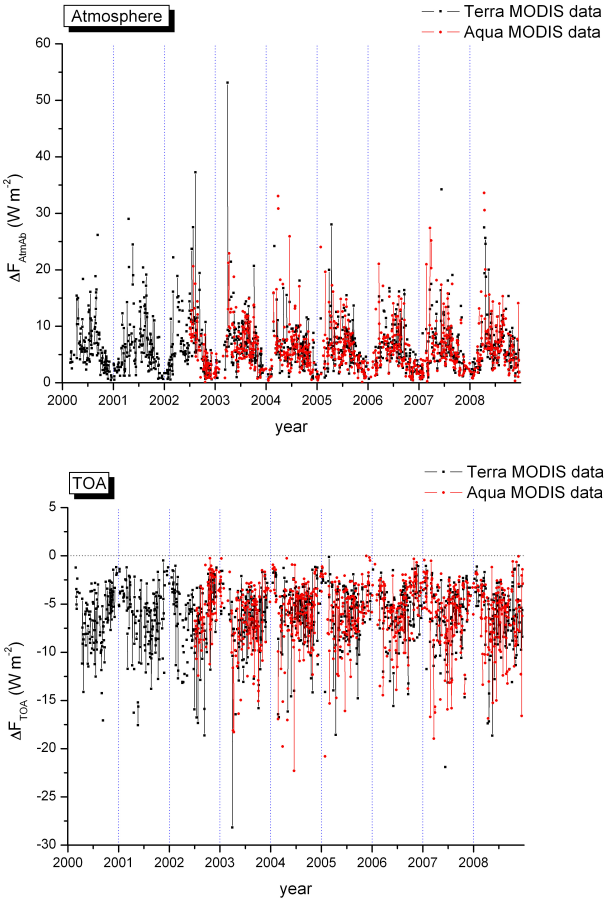

Fig. 10. Time series of the daily mean aerosol effect in the atmosphere **(a)** and at TOA **(b)**, as computed from the model, based on MODIS Level 2 Terra and Aqua data, for the period 2000–2008, at HCMR station, Crete.

ACPD
11, 19881–19925, 2011

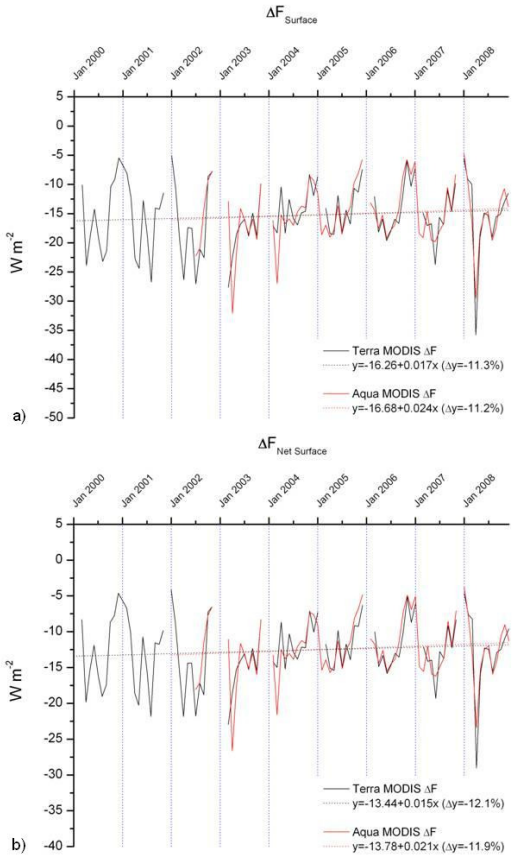

Fig. 11. Time series of the monthly mean aerosol DRE at the surface (incident **(a)** and absorbed **(b)** radiation), as computed from the model, based on Terra and Aqua MODIS Level 2 data, for the period 2000–2008, at HCMR station, Crete. The applied linear fits to the time series are also shown (dotted lines).

ACPD
11, 19881–19925, 2011

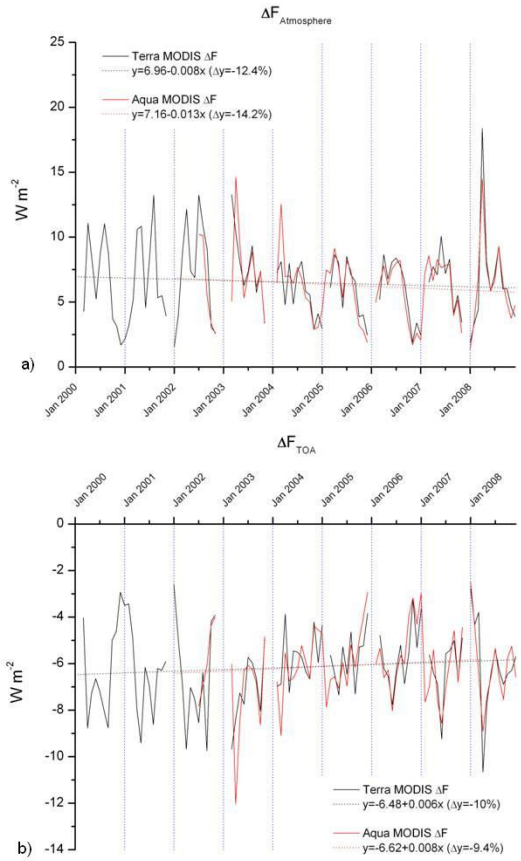

Fig. 12. As in Fig. 11, but for the aerosol DRE within the atmosphere **(a)** and at TOA **(b)**.

ACPD
11, 19881–19925, 2011

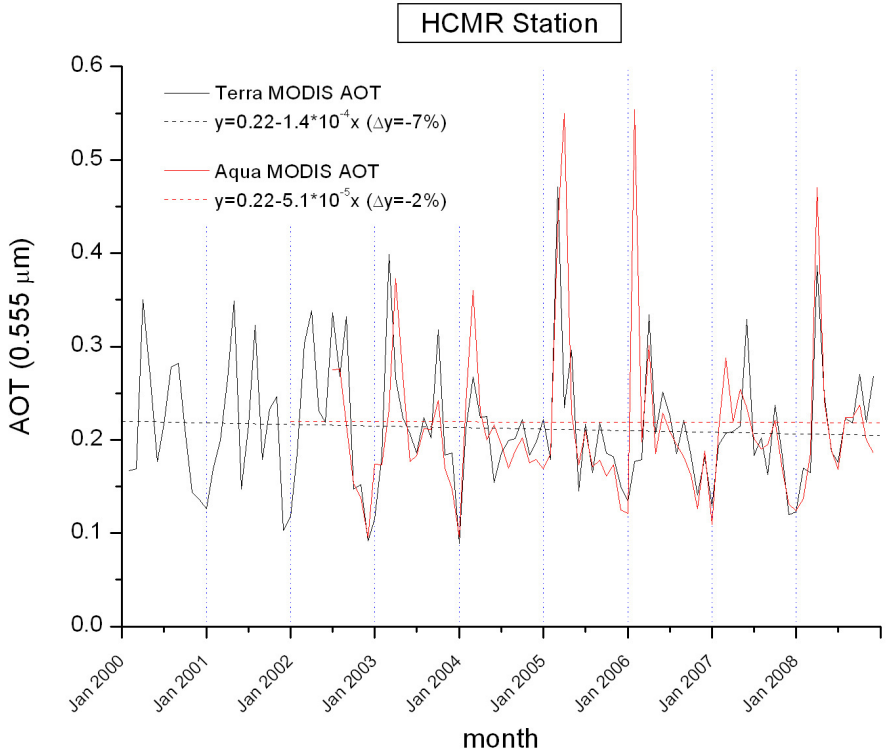

Fig. 13. Time series of the monthly mean AOT at 0.555 μm, based on MODIS Level 2 Terra and Aqua data, for the period 2000–2008, at HCMR station, Crete. The applied linear fits to the time series are also shown (dotted lines).

ACPD
11, 19881–19925, 2011

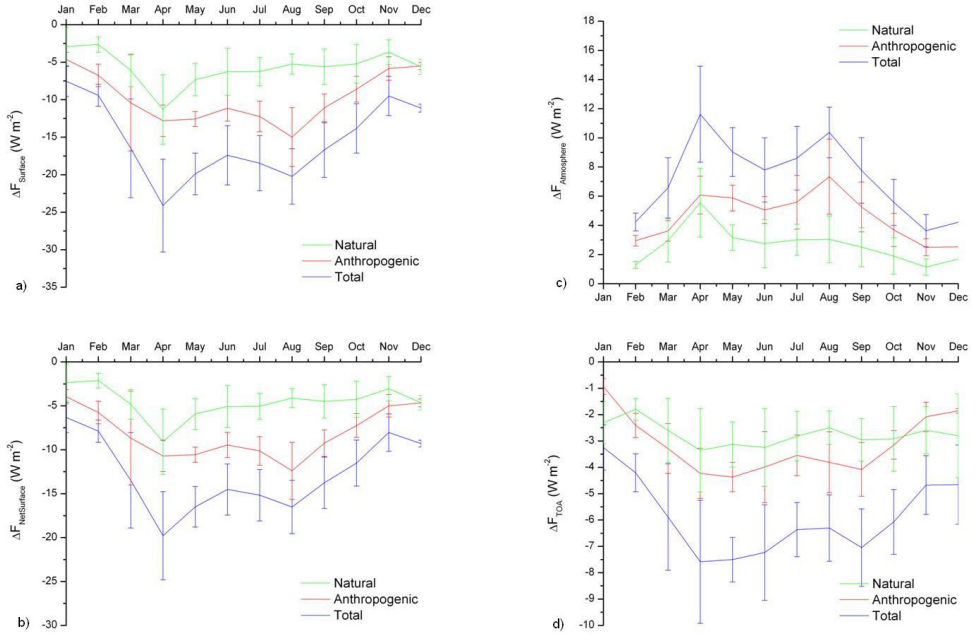

Fig. 14. Mean monthly aerosol DRE and its components (anthropogenic and natural) with standard deviations for the period 2000–2008 **(a)** incident at the surface (HCMR Station), **(b)** absorbed by the surface, **(c)** in the atmosphere and **(d)** at TOA, derived using Terra MODIS data.

ACPD
11, 19881–19925, 2011

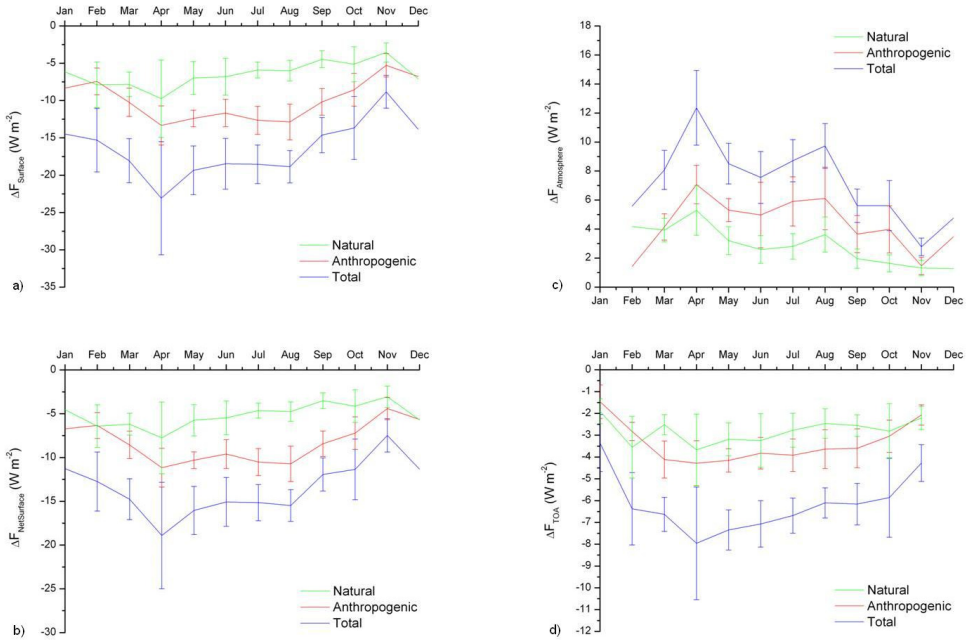

Fig. 15. Mean monthly aerosol DRE and its components (anthropogenic and natural) with standard deviations for the period 2002–2008 **(a)** incident at the surface (HCMR Station), **(b)** absorbed by the surface, **(c)** in the atmosphere and **(d)** at TOA, derived using Aqua MODIS data.

ACPD
11, 19881–19925, 2011